Quantification of Induction Motor Bearing Fault Severity based on Modified Winding Function Theory

Wang, Bingnan; Zhou, Lei; Miyoshi, Masahito; Inoue, hiroshi; Kanemaru, Makoto

TR2021-139   November 23, 2021

Abstract

This paper investigates the accurate modeling of induction motor ball bearing faults using modified winding function method (MWFM). We show that the stator current spectrum can be calculated with the method, and the fault severity of a bearing fault can be quantified with the amplitude of the corresponding faulty current component.

International Conference on Electrical Machines and Systems (ICEMS) 2021

Quantification of Induction Motor Bearing Fault based on Modified Winding Function Method

Bingnan Wang*, Lei Zhou*†, Masahito Miyoshi‡, Hiroshi Inoue‡, and Makoto Kanemaru‡

*Mitsubishi Electric Research Laboratories, 201 Broadway, Cambridge, MA 02139, USA

†Department of Mechanical Engineering, The University of Texas at Austin, Austin, TX, USA

‡Advanced R&D Center, Mitsubishi Electric Corporation, Amagasaki, Japan

Abstract—This paper investigates the analysis and modeling of an induction motor with ball bearing faults based on coupled-circuit model and modified winding function method (MWFM). The impact of the bearing fault is reflected in the variation of air gap profile, and the inductances terms in the coupled-circuit model are calculated and updated for each time step using MWFM. We show that dynamic simulation of an induction motor with bearing fault can be performed with the model, and the stator current spectrum can be calculated to identify the corresponding fault signatures. The method helps quantify bearing fault severity level by monitoring the amplitude of corresponding faulty current components, which facilitates condition-based monitoring of electric machines using motor current signature analysis (MCSA).

I. INTRODUCTION

Induction motors are widely used in numerous industrial applications and factories. Condition monitoring and condition-based maintenance of the machines are becoming more important and desirable in the era of internet of things (IoT). Various mechanical and electrical faults can occur with induction machines, as they could be operating at unfavorable conditions such as high temperature and moisture, and overload; it is therefore valuable to be able to detect the fault before the breakdown of the machines [1], [2]. Among all fault types, bearing fault accounts for about one third of all induction machine failures [3]. Therefore, bearing fault analysis and detection has been an active research area, and sensing mechanisms have been proposed using various signals such as vibration [4], acoustic noise [5], and stator current [1]. Bearing faults impact the mechanical response of the motor system, which is directly reflected in vibration signals and high frequency acoustic noises as well. With established mechanical model, it is possible to identify the fault characteristic frequencies in vibration and acoustic signals, and conduct frequency analysis on the monitored signals to identify the corresponding faults. However, their accuracy often suffers due to the influence of background noises in factory settings, and the sensitivity is largely subject to sensor mounting locations.

Motor current signature analysis (MCSA) is an alternative approach to the fault detection, which collects and analyzes the stator current signals of the motor instead [6], [7], [8]. It has the natural advantages of simple implementation and cost savings, as no additional sensors are required for fault detection. A bearing fault creates an offset of the rotor center, and changes the air gap profile of the motor, which causes a change in air gap permeance and magnetic flux, and eventually is reflected in the stator current signal. The stator current frequency components due to different types of bearing faults can be identified with the bearing geometry and motor speed information [7]. However, bearing fault detection using MCSA method has been mostly performed qualitatively, and fault severity level is difficult to quantify due to the complexity of the motor model. Recently, a quantitative electrical model was proposed aiming to quantify the bearing fault severity level [9], [10]. The relationship of mutual inductance variation induced by the bearing fault, which causes the air gap variation, and corresponding changes of the stator current fault components was theoretically identified. By monitoring the fault components of the stator current, the inductance variation can be identified with the proposed model and used as an indicator for bearing fault severity level. However, the full air gap profile due to bearing fault was not considered in the model, and dynamic simulation of the motor performance with bearing fault cannot be directly conducted.

On the other hand, winding function and modified winding function based coupled-circuit models have been developed for the rapid simulation of motor dynamics, which initially applied to healthy and symmetric motors [11] and later extended to describe various faulty conditions [12], [13]. For coupled-circuit models, the accurate simulation of an induction motor requires accurate calculation of the self and mutual inductances in these coupled circuits. Winding function method was proposed to calculate the inductances using the winding distribution functions and the air gap function which describes the air gap profile for a given rotor position [11]. The inductance calculation method was later improved, hence called modified winding function method (MWFM), to account for the asymmetry caused by mechanical faults [12]. Compared with other equation based methods, such as conventional d-q model, where the windings are assumed to be sinusoidally distributed, MWFM describes the motor dynamics at faulty conditions more accurately, as it considers the actual winding distribution and calculates and updates the time-varying inductances at each time step with the air gap profile at that instance; compared with finite-element simulations, MWFM can calculate the motor dynamics much faster.

In this paper, we develop the quantitative modeling and analysis of an induction machine with bearing faults using

MWFM. Dynamic simulations of the induction machine can be conducted with the developed model to obtain the stator current signals. We will quantify the bearing fault level using faulty signal in the stator current spectrum.

II. Modeling Method

In this section, we first describe the basic formulation of the coupled-circuit model and the calculation of inductances using MWFM [12], then discuss about the modeling of the bearing faults using air gap function.

For a three-phase squirrel-cage induction machine with rotor bar number R, the stator voltage and flux linkage are described by equations

$$V_s = R_s I_s + \frac{\mathrm{d}}{\mathrm{d}t} \Lambda_s, \tag{1}$$

$$\Lambda_s = L_{ss} I_s + L_{sr} I_r, \tag{2}$$

where $V_s = [v_{s1}, v_{s2}, v_{s3}]^\top$ is the stator voltage, $I_s = [i_{s1}, i_{s2}, i_{s3}]^\top$ is the stator current, $\Lambda_s = [\lambda_{s1}, \lambda_{s2}, \lambda_{s3}]^\top$ is the stator flux linkage, $I_r = [i_{r1}, i_{r2}, ..., i_{rR}, i_e]^\top$ is a vector of length $R+1$ to describe rotor loop currents and the end ring current respectively. R_s is a 3×3 stator resistance matrix, L_{ss} is the 3×3 stator inductance matrix, and L_{sr} is the $3 \times (R+1)$ matrix containing mutual inductances between stator phases and rotor loops.

For the rotor side, the voltage equation and flux linkage equation are respectively

$$V_r = R_r I_r + \frac{\mathrm{d}}{\mathrm{d}t} \Lambda_r, \tag{3}$$

$$\Lambda_r = L_{rs} I_s + L_{rr} I_r, \tag{4}$$

where $L_{rs} = L_{sr}^\top$, and L_{rr} is the $(R+1) \times (R+1)$ self-inductance matrix of the rotor loops. Note that for squirrel cage rotors, the rotor voltages are zero: $V_r = [0, 0, ..., 0]^\top$.

For a three-phase IM with Y-connection, the input signals are the line-to-line voltages. Transforming the stator voltage equation (1) into line-to-line voltage input we have

$$V_{sl-l} = \begin{bmatrix} v_{s1} - v_{s2} \\ v_{s2} - v_{s1} \\ v_{s3} - v_{s1} \end{bmatrix}$$
$$= \begin{bmatrix} r_s & -r_s & 0 \\ 0 & r_s & -r_s \\ -r_s & 0 & r_s \end{bmatrix} I_s + \frac{\mathrm{d}}{\mathrm{d}t} \begin{bmatrix} \lambda_{s1} - \lambda_{s2} \\ \lambda_{s2} - \lambda_{s3} \\ \lambda_{s3} - \lambda_{s1} \end{bmatrix} \tag{5}$$

The torque equation of the induction motor is

$$T_e = \frac{1}{2} I_s^\top \frac{\partial L_{ss}}{\partial \theta_r} I_s + I_s^\top \frac{\partial L_{sr}}{\partial \theta_r} I_r + \frac{1}{2} I_r^\top \frac{\partial L_{rr}}{\partial \theta_r} I_r, \tag{6}$$

where θ_r is the rotor's mechanical angle.

The mechanical dynamics of the motor is

$$\frac{\mathrm{d}}{\mathrm{d}t} \omega_r = \frac{1}{J}(T_e - T_L), \tag{7}$$

$$\frac{\mathrm{d}}{\mathrm{d}t} \theta_r = \omega_r, \tag{8}$$

where ω_r is the mechanical speed, T_L is the load torque, and J is the inertia of the rotor.

As we can see from the model, it is critical to calculate the inductance components in equations (2) and (4), and the inductance derivatives in equation (6).

The MWFM is used to calculate the motor's inductance matrices. The inductance between a pair of windings at each time step can be calculated by the integration of the product of the two winding functions and the air gap permeance function, over all stator angles. For winding i and winding j, the inductance is derived as

$$L_{ij}(t) = \mu_0 lr \int_0^{2\pi} n_i(\phi, t) M_j(\phi, t) g^{-1}(\phi, t) \mathrm{d}\phi, \tag{9}$$

where μ_0 is the vacuum permeability, r is air gap radius, l is the stack length, $n_i(\phi, t)$ is the winding turns function for winding i, and $M_j(\phi, t)$ is the modified winding function for winding j, which is calculated by

$$M(\phi, t) = n(\phi, t) - \left\langle M(t) \right\rangle, \tag{10}$$

where

$$\left\langle M(t) \right\rangle = \frac{1}{2\pi \langle g^{-1}(\phi, t) \rangle} \int_0^{2\pi} n(\phi, t) g^{-1}(\phi, t) \mathrm{d}\phi, \tag{11}$$

$$\left\langle g^{-1}(\phi, t) \right\rangle = \frac{1}{2\pi} \int_0^{2\pi} g^{-1}(\phi, t) \mathrm{d}\phi. \tag{12}$$

For dynamic simulation of the induction motor, the inductance terms are updated at each time step. Coupled with the voltage, flux linkage, torque, and mechanical dynamics equations from (1) to (8), the full dynamic performance of the induction motor can be obtained.

Next we show how the bearing faults come into play and eventually present in the stator current signals.
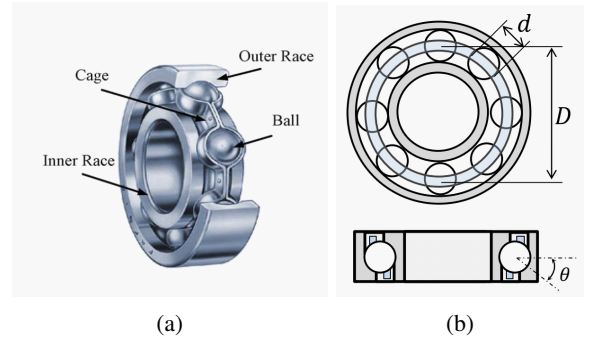

Fig. 1: (a) Structure of a ball bearing and (b) the cross sectional view with geometric parameters.

For a typical ball bearing, the structure is illustrated in Fig. 1(a), which has an outer race mounted on the motorcap, an inner race that holds the motor shaft, rolling elements or balls to reduce the friction between the rotating and stationary parts, and a cage to restrain the relative locations of the rolling elements. A side view and a top view of the ball bearing structure is shown in Fig.Fig. 1(b). A few key parameters are also labeled in the figure, which will be used to describe the characteristic frequencies of bearing faults: D is the diameter of the bearing measured between the center of raceway; d is

the diameter of each ball in the bearing; and θ describes the contact angle between the ball and the raceway. When there is a defect at certain locations of the bearing, the rotation will not be smooth anymore, and periodic vibration pulses will be generated while the motor is rotating. Depending on the specific location of the fault, the corresponding characteristic frequency f_c can be identified based on the geometry of the bearing and the rotation speed of the machine. With the motor rotation frequency f_r and bearing geometrical parameters labeled in Fig. 1(b), where the point of contact between the ball and the raceway is characterized by the contact angle θ, the common fault types and the corresponding characteristic frequencies are given by:

Cage defect hits outer race: $\quad f_{co} = \dfrac{f_r}{2}\left(1 - \dfrac{d}{D}\cos\theta\right)$

Cage defect hits inner race: $\quad f_{ci} = \dfrac{f_r}{2}\left(1 + \dfrac{d}{D}\cos\theta\right)$

Outer race defect hits balls: $\quad f_o = N_b\dfrac{f_r}{2}\left(1 - \dfrac{d}{D}\cos\theta\right)$

Inner race defect hits balls: $\quad f_i = N_b\dfrac{f_r}{2}\left(1 + \dfrac{d}{D}\cos\theta\right)$

Ball defect hits both races: $\quad f_b = \dfrac{D}{d}f_r\left(1 - \dfrac{d^2}{D^2}\cos^2\theta\right)$

In general, when a point defect comes into contact with another bearing element causes a radial displacement of the rotor center, or eccentricity. At that instance, the air gap profile described by $g(\phi, t)$ is changed due to the defect, hence the permeance, which is inversely proportional to the inverse of the air gap, is also modified. As a result, the mutual inductance between stator winding and rotor loop is affected according to equation (9). With the dynamic model of the induction motor, additional frequency components in the stator current spectrum at $|f_s \pm n \cdot f_c|$ will be present due to the fault, with f_s being the fundamental electrical frequency.

Detailed description of the air gap profile caused by a specific type of bearing fault has been given in Ref. [7]. The periodic modification of the air gap length due to bearing fault caused eccentricity is modeled by a series of Dirac delta functions that is commonly used in vibration analysis. In the presence of a bearing fault, the air gap profile of a motor at stator angle ϕ and time t is described by

$$g(\phi, t) = g_0\left[K_c - e_0\cos(\phi + \psi(t))\sum_{k=-\infty}^{+\infty}\delta\left(t - \frac{k}{f_c}\right)\right],\tag{13}$$

where g_0 is the nominal air gap length, K_c is the carter's coefficient to account for the increase of effective air gap length due to slotting effect, e_0 is the eccentricity level caused by the bearing fault, and $\psi(t)$ is the defect position. In practical implementation of the model, rectangular shaped pulses with finite width, instead of those described by Dirac delta functions, are often used for the analysis of bearing faults [14], [15]. Depending on the fault type, the defect position have different time dependence. For outer race fault, the fault position is fixed, since outer race always stays in place, hence $\psi(t) = 0$ for all time instances. For inner race

fault, the fault rotates with the inner race and rotor, and the movement is $\psi(t) = 2\pi f_r t$. The time-dependence of inner race fault is illustrated in Fig. 2. The inner race rotates with the rotor at the same rotation frequency f_r, the outer race stays still, while each ball in the bearing rotates between inner and outer race. At time instance t_1, the fault is located at $\psi(t_1)$; there is no contact between the inner race fault and any balls in the bearing, and the inner race is centered. After some time, at time instance t_2, the fault rotates to a new location at $\psi(t_2)$; a ball marked in red color came in contact with the inner race fault, causing a shift of the rotation center, therefore the whole air gap profile along the circumference is changed. The maximum of the air gap variation created by the fault is quantified as $g_0 e_0$.
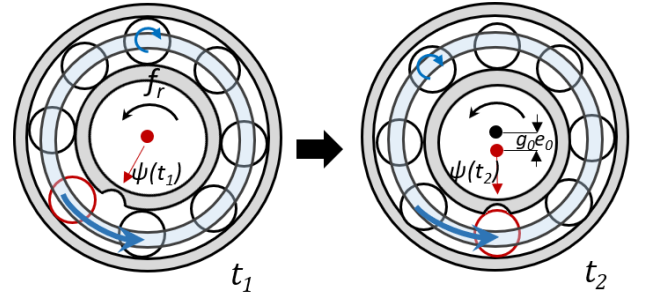

Fig. 2: Illustration of a bearing with inner race fault, when (a) there is no contact between the fault and a ball, and (b) when the fault is in contact with a ball.

III. RESULTS & DISCUSSIONS

In this paper, a 1-hp induction machine is studied, with key parameters listed in Table I. Two 6022-ZZ bearings mounted on the load side and the opposite side respectively, with each bearing has 8 balls. The inner race defect characteristic frequency is approximately $f_i \approx 0.6nf_r = 4.8f_r$, while an outer race defect gives characteristic frequency of $f_o \approx 0.4nf_r = 3.2f_r$.

TABLE I: Major Parameters of the Induction Motor

Parameter	Value
Number of pole pairs	2
Number of bars	28
Number of stator slots	36
Number of turns per slot	37
Nominal air gap length g_0	0.28 mm
Air gap radius r	41.6 mm
Stack length l	80 mm
Carter's coefficient K_c	1.40

We model the induction motor with an inner race fault, in which case the air gap profile is described by equation (13), with fault angular position rotates as function of time: $\psi(t) = 2\pi f_r t$. Assume the fault causes a eccentricity level $e_0 = 0.3$, the air gap length as function of the stator angle is plotted in Fig. 3. When there is no contact between the fault and any ball in the bearing, the air gap is constant; when

there is contact, a static eccentricity effect is created. Here the air gap is normalized to its nominal length, and the Carter's coefficient, with value listed in Table I, is included to account for the slotting effect.

Note that the exact shape and width of the pulses created by a specific bearing fault to the change of air gap profile are often difficult to predict with mechanical model of the motor as there are many degrees of freedom involved, or verify with experimental measurements. Therefore, the MWFM based simulation model offers a way to connect the air gap profile to the specific fault features in the obtained stator current spectrum for each type and severity level of bearing fault, which can be compared with experimental results to identify the fault type exists in the bearings, and quantify the severity of each fault. In the following simulations, we assume an inner race fault creates rectangular pulses to the air gap profile, with duty cycle of 0.5.
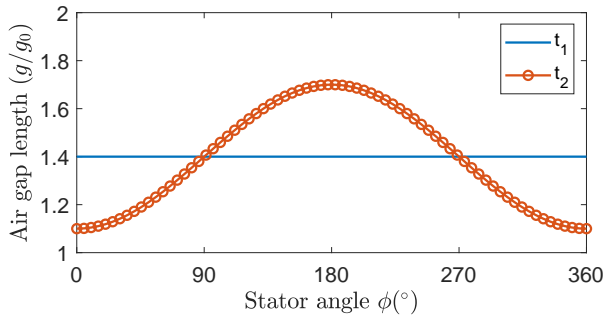

Fig. 3: Normalized air gap profile as a function of stator angle for in the case of inner race fault, when there is no contact between fault and a ball, and when there is contact, which corresponds to the illustration of Fig. 2, with eccentricity level $e_0 = 0.3$ assumed.

With the air gap profile at each condition, and the model established in the previous section, we can conduct dynamic simulation of the motor operation. We simulated the induction motor with healthy bearing, and faulty bearing with inner race fault, both at no load conditions. For the faulty case, we assume an eccentricity level $e_0 = 0.3$ is created to the air gap variation, which corresponds to Fig. 3. With the line voltage of 200 V and line frequency of $f_s = 60$ Hz, the phase current as function of time is simulated and plotted in Fig. 4. As seen from the enlarged plot in Fig. 4(b), the time-domain signals are dominated by the fundamental component, but there are small features in each curve, with the faulty case seem to have more components. To understand the details, Fourier transform is applied to obtain the spectrum of the two cases, and the results are shown in Fig. 5. Due to the inner race fault with characteristic frequency $f_c = 144$ Hz, we observe fault signatures at $f_c - f_s = 84$ Hz and $f_c + f_s = 204$ Hz in the current spectrum, which are missing in the case of healthy bearings.

For the MWFM based model, any mechanical fault is described in the air gap profile. Therefore, we can also quantitatively evaluate the relation of the fault severity, which causes different level of air gap variation, and the
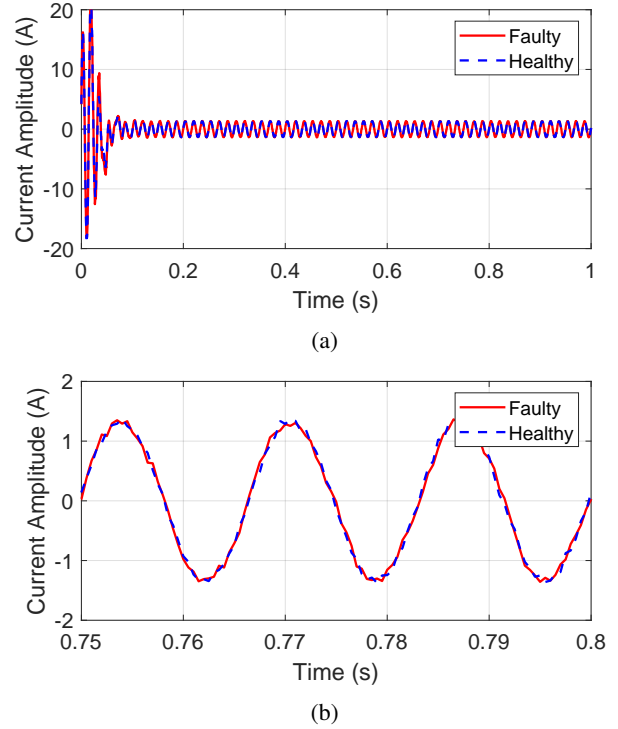

Fig. 4: (a) Simulated stator current signal the induction motor with healthy bearing ($e_0 = 0$, blue dashed curve), and inner race fault with $e_0 = 0.3$ (red curve), with a zoom-in plot shown in (b).
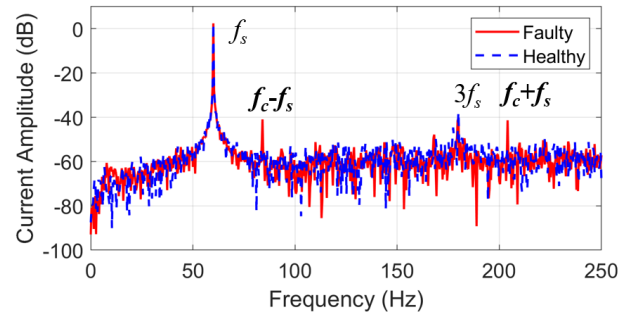

Fig. 5: Simulated current spectrum of the induction motor with healthy bearing ($e_0 = 0$, blue dashed curve), and inner race fault with $e_0 = 0.3$ (red curve). f_c and f_s are the fault and supply frequency respectively.

corresponding faulty component amplitude in the phase current spectrum. Fig. 6 shows the amplitude of the two lowest order fault components at $f_c - f_s$ and $f_c + f_s$ due to the inner race fault, normalized to the fundamental component at f_s, as a function of the eccentricity level caused by the fault. As expected, the amplitude increases monotonically with the increasing fault level. In fact, the amplitude of the fault component is proportional to the corresponding magnetic flux component generated due to the fault. Since the magnetic flux is the product of the air gap permeance and the rotor generated MMF, both of which are linearly proportional to the fault level, the fault current component should be a quadratic

function of the fault level. In Fig. 6, we fit each of the two fault components with a quadratic function $y = ax^2 + b$ to show the trend of amplitude growth with increasing fault level. The fitting coefficients are $a = 0.0761$, $b = 0.0002$ for $f_c - f_s$ component, and $a = 0.0849$, $b = 0.0002$ for $f_c + f_s$ component.
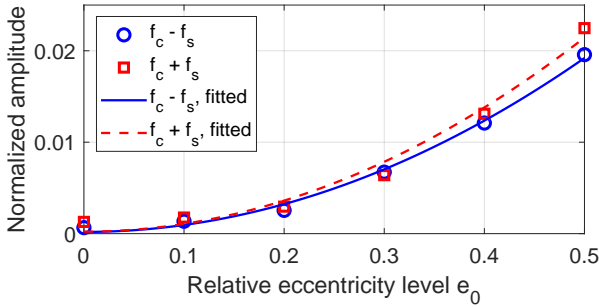

Fig. 6: Simulated faulty current amplitude at $f_c - f_s$ and $f_c + f_s$, normalized to the fundamental current at f_s, as a function of the eccentricity level e_0, with fitted curves using quadratic function $y = ax^2 + b$ are also shown.

Such fault analysis is helpful in identifying and quantifying the signatures due to various faults. For condition monitoring and condition-based maintenance of electric machines based on MCSA, we envision that fault components in the stator current of the machines that correspond to different fault types are regularly monitored and compared against pre-determined threshold values; maintenance requests for corresponding faulty components are triggered if the monitored fault indicators exceed the threshold values. To achieve that, proper threshold values need to be identified for each component and each electric machine. As there can be many machines of different power ratings that are operating at the same plant, each with varying speed and load conditions, the fault component values for different machines and different conditions also vary. The quantitative MWFM based model includes the electrical parameters of the electric machine, accounts for different mechanical faults with changing air gap profile, and can simulate the dynamic operation of electrical machine with different load conditions. Although only the result with inner race fault is demonstrated in the paper, it is straightforward to evaluate other bearing fault conditions, or a combination of multiple faults.

IV. CONCLUSIONS

In this paper, we investigated the dynamic modeling of induction motor with ball bearing faults based on coupled-circuit model and modified winding function method (MWFM). The mechanical fault is described by the the modulation of the air gap profile of the motor. We showed that the stator current spectrum can be obtained with the model, and fault signatures of bearing faults can be identified and quantified. For motor condition monitoring and condition-based maintenance using motor current signature analysis (MCSA) method, this model helps identify the fault severity and set proper threshold values for maintenance needs.

REFERENCES

[1] M. El Hachemi Benbouzid, "A review of induction motors signature analysis as a medium for faults detection," *IEEE Transactions on Industrial Electronics*, vol. 47, no. 5, pp. 984–993, 2000.

[2] P. Zhang, Y. Du, T. G. Habetler, and B. Lu, "A survey of condition monitoring and protection methods for medium-voltage induction motors," *IEEE Transactions on Industry Applications*, vol. 47, no. 1, pp. 34–46, 2011.

[3] "Report of large motor reliability survey of industrial and commercial installations, part i," *IEEE Transactions on Industry Applications*, vol. IA-21, no. 4, pp. 853–864, 1985.

[4] J. Harmouche, C. Delpha, and D. Diallo, "Improved fault diagnosis of ball bearings based on the global spectrum of vibration signals," *IEEE Transactions on Energy Conversion*, vol. 30, no. 1, pp. 376–383, 2015.

[5] M. Kang, J. Kim, and J.-M. Kim, "An fpga-based multicore system for real-time bearing fault diagnosis using ultrasampling rate ae signals," *IEEE Transactions on Industrial Electronics*, vol. 62, no. 4, pp. 2319–2329, 2015.

[6] R. Schoen, T. Habetler, F. Kamran, and R. Bartfield, "Motor bearing damage detection using stator current monitoring," *IEEE Transactions on Industry Applications*, vol. 31, no. 6, pp. 1274–1279, 1995.

[7] M. Blodt, P. Granjon, B. Raison, and G. Rostaing, "Models for bearing damage detection in induction motors using stator current monitoring," *IEEE Transactions on Industrial Electronics*, vol. 55, no. 4, pp. 1813–1822, 2008.

[8] W. Zhou, T. G. Habetler, and R. G. Harley, "Bearing fault detection via stator current noise cancellation and statistical control," *IEEE Transactions on Industrial Electronics*, vol. 55, no. 12, pp. 4260–4269, 2008.

[9] S. Zhang, B. Wang, M. Kanemaru, C. Lin, D. Liu, K. H. Teo, and T. G. Habetler, "Quantification of rolling- element bearing fault severity of induction machines," in *2019 IEEE International Electric Machines Drives Conference (IEMDC)*, 2019, pp. 44–50.

[10] S. Zhang, B. Wang, M. Kanemaru, C. Lin, D. Liu, M. Miyoshi, K. H. Teo, and T. G. Habetler, "Model-based analysis and quantification of bearing faults in induction machines," *IEEE Transactions on Industry Applications*, vol. 56, no. 3, pp. 2158–2170, 2020.

[11] X. Luo, Y. Liao, H. A. Toliyat, A. El-Antably, and T. A. Lipo, "Multiple coupled circuit modeling of induction machines," *IEEE Transactions on industry applications*, vol. 31, no. 2, pp. 311–318, 1995.

[12] N. Al-Nuaim and H. Toliyat, "A novel method for modeling dynamic air-gap eccentricity in synchronous machines based on modified winding function theory," *IEEE Transactions on Energy Conversion*, vol. 13, no. 2, pp. 156–162, 1998.

[13] L. Zhou, B. Wang, C. Lin, H. Inoue, and M. Miyoshi, "Static eccentricity fault detection for psh-type induction motors considering high-order air gap permeance harmonics," in *2021 IEEE International Electric Machines Drives Conference (IEMDC)*, 2021, pp. 1–7.

[14] P. McFadden and J. Smith, "Model for the vibration produced by a single point defect in a rolling element bearing," *Journal of Sound and Vibration*, vol. 96, no. 1, pp. 69–82, 1984.

[15] N. Tandon and A. Choudhury, "An analytical model for the prediction of the vibration response of rolling element bearings due to a localized defect," *Journal of Sound and Vibration*, vol. 205, no. 3, pp. 275–292, 1997.